

## ■ Biological Chemistry &amp; Chemical Biology

## Subcellular Optical pH Nanoscale Sensor

Manuel García-Algar,<sup>[a]</sup> Dionysia Tsoutsis,<sup>[b]</sup> Marcos Sanles-Sobrido,<sup>[b, c]</sup> Andreu Cabot,<sup>[c, d]</sup> Victor Izquierdo-Roca,<sup>[c]</sup> and Habil. Pilar Rivera Gil<sup>\*[b]</sup>

Coated gold nanoparticles bearing a pH-sensitive molecule serve as nanoscale optical sensors for non-invasive pH quantification of their endocytosis through surface-enhanced Raman scattering. Our sensor consists in colloidal gold spheres coated either with (polyethylene glycol) PEG molecules or a silica shell. They carry a sensor molecule that specifically recognize protons. The read out for monitoring changes in the pH is the Raman shift of the sensor molecule that is enhanced on the surface of the plasmonic spheres. Sensing was performed along the way of internalization from the extracellular site through different endo/lysosomal compartments where they are closely packed. The creation of hot spots favored by particle agglomeration inside cells was responsible for the enhancement of changes in signal intensity and was dependent on the surface chemistry. We establish a correlation between the physicochemical properties of the nanoscale sensor (shape, surface chemistry) and its ability to monitor the different pH along its cellular internalization. The PEGylated spheres can sensitively track the pH along their cellular internalization whereas the silica coated ones fail.

Control of ion homeostasis is essential for all cellular organisms. At physiological condition, ions like  $K^+$  or  $H^+$  are found at high concentrations inside the cells, whereas ions like  $Na^+$ ,  $Ca^{2+}$ , or  $Cl^-$  are rather found extracellularly.<sup>[1]</sup> Many pathological situations are associated with a defective regulation of the ion concentrations.<sup>[1,4]</sup> For example, disregulation of the  $K^+$  entry

might alter  $Ca^{2+}$  homeostasis; thus, leading to neuronal degeneration and all associated diseases like Alzheimer, stroke or ischemia, and epilepsy.<sup>[5]</sup> In Alzheimer, Parkinson or prion diseases, metal ions such as  $Cu^{2+}$ ,  $Zn^{2+}$  or  $Fe^{3+}$  influence the kinetics of amyloid fiber formation and neurotoxicity.<sup>[6]</sup> Multiple sclerosis has traditionally been considered an inflammatory disorder, however in the last years an abnormal distribution of ion channels<sup>[7]</sup> and  $Ca^{2+}$  imbalances has been directly associated with neuronal degeneration.<sup>[8]</sup> Alterations in the homeostasis of lysosomal pH have been associated with several forms of lysosomal storage disorders.<sup>[9]</sup> Understanding the mechanisms of pathogenesis of these diseases is crucial to find new targets for effective pharmaceuticals. Monitoring the dysregulation of ion homeostasis plays a key role in this understanding. So far most of the techniques employed to measure ion concentrations make use of electrodes<sup>[10]</sup> or fiber-based optodes.<sup>[11,12]</sup> These systems work well for solutions but in general not for cellular organisms, since they are too big to enter the cells over extended periods of time. There are other techniques like microanalysis that can measure intracellular analyte concentrations. However, they are destructive for the biological sample.<sup>[13]</sup> For subcellular (intracellular) analyte detection smaller non-invasive sensors are required, especially if long term measurements in live cells are envisaged. One possibility toward this direction is the use of nano/microparticles that carry analyte-sensitive molecules.<sup>[14,15]</sup> Examples of such nano/micrometer-sized containers include the PEBBLE (Probes Encapsulated By Biologically Localized Embedding) system extensively described by the Kopelman group in the last decade,<sup>[16]</sup> solid particle matrices,<sup>[17]</sup> liposomes,<sup>[18]</sup> hollow fiber membranes,<sup>[19]</sup> vesicles,<sup>[20]</sup> and polyelectrolyte capsules.<sup>[9,21]</sup> Carriers must be designed in a way that ions can freely diffuse to the location of the sensor. Since several sensor molecules can be adsorbed to the carrier, an increase in the detection efficiencies with respect to individual molecular sensors can be achieved. Furthermore, the incorporation of the molecular sensors to the particle avoids problems such as delocalization or various non-specific interactions. The sensors transduce the chemical information into a readout signal. This signal may be highly localized in subcellular compartments where the carriers are, but it must be externally accessed. Most optical signals, particularly fluorescence, are used as read-out because of their ease of remote detection, but electrochemical read outs making use of proper electrodes has also been described.<sup>[22]</sup> Several important disadvantages have recently raised concern about the technological applicability of fluorescent-based sensors. Such limitations include photobleaching of the sensor

[a] M. García-Algar

Department of Physical and Inorganic Chemistry,  
Rovira I Virgili University,  
Catalonian Centre for Technological Chemistry (CTQC) and Medcom Advance S.L.

Carrer Marcel·li Domingo s/n, 43007 Tarragona, Spain

[b] Dr. D. Tsoutsis, Dr. M. Sanles-Sobrido, Dr. H. P. R. Gil

Integrative Biomedical Materials and Nanomedicine Lab,  
Department of Experimental and Health Sciences,  
Universitat Pompeu Fabra

Carrer Doctor Aiguader 88, Barcelona, Spain

E-mail: pilar.rivera@upf.edu

[c] Dr. M. Sanles-Sobrido, Prof. A. Cabot, Dr. V. Izquierdo-Roca

Catalonia Institute for Energy Research (IREC)  
Jardins de les Dones de Negre 1, 08930 Sant Adrià de Besòs, Barcelona,  
Spain

[d] Prof. A. Cabot

ICREA, Pg.

Lluís Companys 23, 08010 Barcelona, Spain



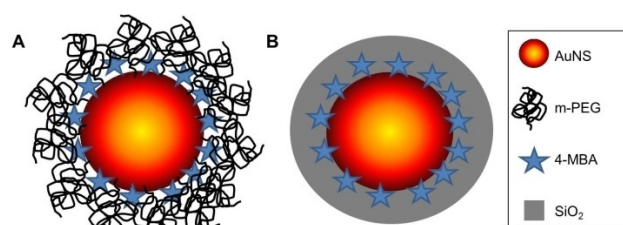
Supporting information for this article is available on the WWW under  
<https://doi.org/10.1002/slct.201701087>

molecule, limited multiplex possibilities linked to the spectral resolution of the emission wavelengths of the dyes and chemical destruction of the sensor inside cells. Although there are tricks to circumvent these complications,<sup>[23]</sup> adequate active optical materials with a more reliable read out are required. Much more selective and sensitive colloidal sensors which make use of the spectroscopic response of the adsorbate at the surface of metallic nanoparticles, an effect known as surface-enhanced Raman scattering (SERS) have recently been described.<sup>[24–25]</sup> However, the feasibility of this technique for the real time monitoring of the dynamics of ions inside cells in a non-invasive manner has not been proven yet. Some nanostructured needles have been created for SERS measurements inside cells, however they cannot target at the subcellular level and they have an extremely low throughput. We very recently described an approach towards the local quantification of nitric oxide inside living cells.<sup>[26]</sup> This approach involved plasmonic gold nanocapsules showing excellent biocompatibility and signal-to-noise ratio while at the same time overcoming the aforementioned limitations.<sup>[26]</sup> Other works also showed SERS-mediated pH sensing on cells, however they either used silver,<sup>[27]</sup> thus being potentially toxic or intentionally agglomerate the nanoparticles,<sup>[28–29]</sup> thus probably having polydispersity problems and irreproducible SERS issues. Other located the Raman probe close to the negatively charged stabilizing groups,<sup>[30]</sup> thus creating an ionic environment different from the bulk.

Motivated by these challenges and the report of gold nanoparticles for the SERS detection of pH values at the level of single plasmonic nanoparticles<sup>[24]</sup> and by our previous results on colloidal non-invasive sensors for the *in situ*, real time monitoring of ion imbalances at the subcellular level,<sup>[26]</sup> we created a biofriendly, colloidal stable pH optical sensor to quantify at real time their cellular internalization in live cells. Endocytosis is a pH dependent biological process. Gold nanoparticles were synthesized and labeled with 4-mercaptobenzoic acid (4-MBA) that served as Raman probe and as pH sensing molecule. This probe transduces local changes of pH into modifications on its SERS vibrational spectra. Such pH sensitivity can in turn help to track these nanoparticles inside living cells. The colloidal sensors were coated with mercapto-polyethylene glycol (m-PEG) or with a porous silica (SiO<sub>2</sub>) shell to reduce absorption of proteins or other macromolecules present on cell medium, which could affect the sensitivity of the pH sensor. Two different coatings were used to determine the influence of the surface chemistry on the interaction with the cells and ultimately on the performance of the sensor. The intracellular pH was then non-invasively quantified inside cells.

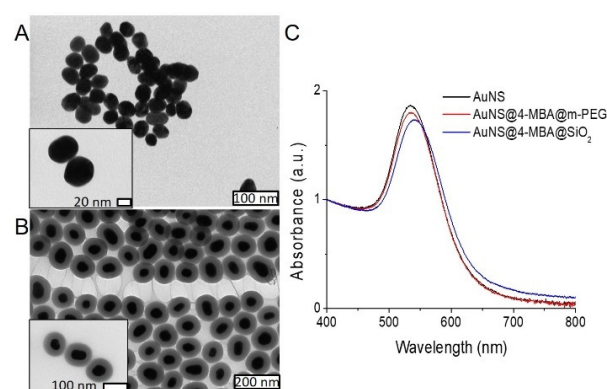
## Synthesis and characterization of AuNS

Figure 1.A and 1.B show a schematic representation of the gold nanospheres (AuNS) under study. They consist of a gold core capped with two different stabilizers, m-PEG or silica shell, and 4-MBA as pH sensor molecule. Affinity of the mercapto group, from m-PEG and 4-MBA, for gold makes possible the physical attachment of the compounds to the surface of gold core.



**Figure 1.** Schematic representation of Au NanoSpheres (AuNS) labeled with 4-MBA and coated with (A) mercapto-polyethyleneglycol (m-PEG), as stabilizer of the particles in water and (B) with porous silica (SiO<sub>2</sub>) shell. Figure not drawn to scale.

Transmission electron microscopy (TEM) images of the AuNS synthesized and used in this work (Figure 2.A) confirm a



**Figure 2.** TEM images of (A) as synthesized 50 nm diameter AuNS in water and of (B) AuNS after coating with 30 nm layer of silica. (C) UV-Vis absorption spectra of bare AuNS (black line), AuNS with 4-MBA and m-PEG (red line) and with silica coating (blue line).

controlled particle size from 43–56 nm in a homogeneous distribution throughout the sample. In the same way, Figure 2.B shows the AuNS after silica coating. A layer of 30 nm of silica was formed around the majority of AuNS in a homogeneous distribution. Well-shaped and isolated core-shell structures can be seen in Figure 2.B. Optical properties of the as synthesized nanoscaled sensors (*i.e.* AuNS@4-MBA@m-PEG and AuNS@4-MBA@SiO<sub>2</sub>) depend on their structural parameters and the immediate dielectric environment,<sup>[31]</sup> which directly involves the components surrounding the surface of material. Figure 2.C shows the localized surface plasmon resonance (LSPR) band located at 534 nm for the bare and m-PEG coated AuNS. After silica coating of the AuNS, the corresponding LSPR band is slightly red-shifted at 539 nm due to the different refractive index of the silica shell.

## Particle uptake and subcellular distribution

Surface modification of the colloidal sensors with different coatings affects their interactions with eukaryotic cells and may

have an influence on their performance. Exposure of both pH sensors (AuNS@4-MBA@m-PEG and AuNS@4-MBA@SiO<sub>2</sub>) to SK-BR-3 cells, denote a good tolerance of cells to both particles. Observations based on cell morphology at individual and culture level, suggest great compatibility without negative interference on the cell integrity. Figure 3 shows confocal

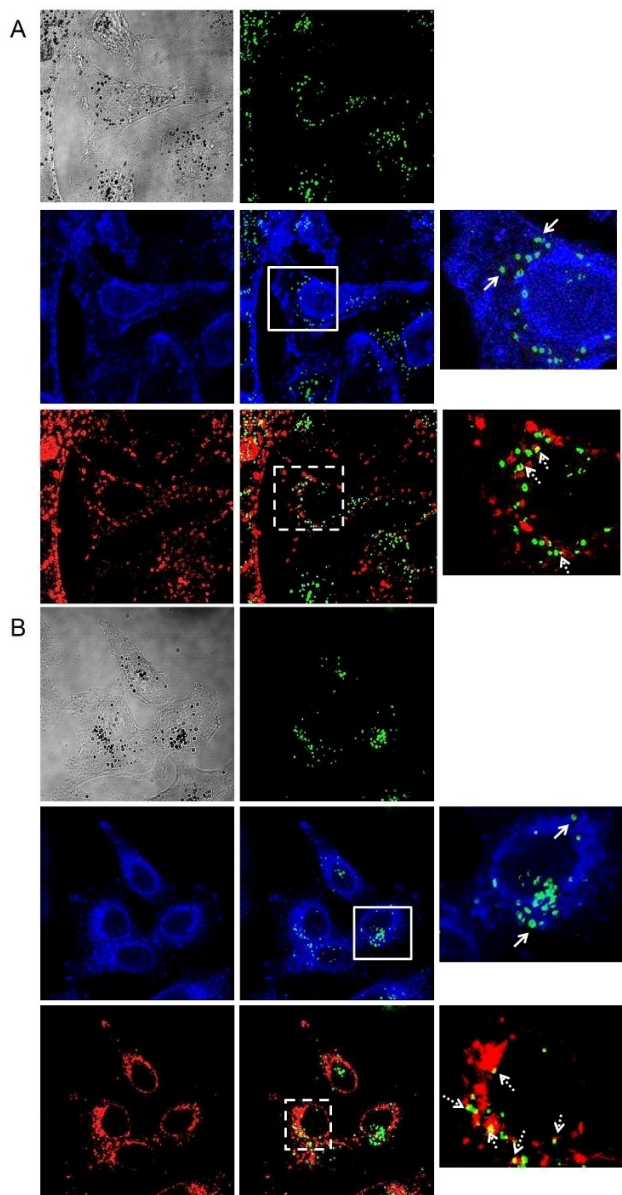


**Figure 3.** Confocal laser scanning microscopy images of SK-BR-3 cells after 24 h incubation with (a) AuNS@4-MBA@m-PEG and (b) AuNS@4-MBA@SiO<sub>2</sub>. The figure shows particles in green, cell membranes in blue, and the lysosome in red. White solid arrows show examples of the sensors at the plasma membrane. Dashed arrows show example of sensors colocalizing with the lysosomes.

microscope images of both capped sensors distributed inside the cells in a punctuate manner after 24 h. We found more PEG-coated particles interacting with the cells than silica-coated. Despite it is known that PEG adsorbates reduce particle

uptake in comparison with other organic molecules,<sup>[32]</sup> we did not observe a lack of internalization. This can be due to the small size of the PEG (1 kDa) used in this work in comparison to other works using 10 kDa PEGs to reduce particle recognition and uptake.<sup>[33–34]</sup>

Additionally, internalization events take place as earlier as 30 min, so that after 24 h a high number of 4-MBA@m-PEG capped particles are incorporated. Figure 3.A and 3.B show the particles surrounded by the cell membrane (stained in blue) and partially co-localizing with the lysosomes (stained in red). The particles are shown in green, due to the reflected light from the gold core upon illumination. For both AuNS@4-MBA@m-PEG and AuNS@4-MBA@SiO<sub>2</sub>, fluorescence from lysosome and from particles are co-localizing at the same place and were collected near nuclei. All this suggest endocytosis as mechanism of internalization, and a perinuclear localization within the lysosomes, as the final fate for both sensors; however, with a different internalization pattern. Furthermore, a strong signal was found at the level of the plasma membrane for the silica coated sensors. Therefore, agglomeration of the particles outside the cells cannot be excluded for this kind of particles.

**The colloidal pH meter.** During the process of endocytosis, the different vesicles involved continuously lower their pH by fusing with acidic structures until reaching their final destination, which is normally the lysosome. Lysosomal pH has been described about 5 or less and is the most acidic vesicle inside the cell. The cells actively internalized our sensors and transport them through the different endocytic vesicles, therefore they can be used as local reporters for the internalization process. The idea is to perform a live quantification of the pH of the vesicles where they reside during their uptake and intracellular distribution. This will have an impact on monitoring the dynamics of protons on altered cells affecting diseases such as lysosomal storage disorders. To test the responsiveness and the strength of the sensors, particles were suspended in different media which pH was adjusted from 1 to 12 and the optical response was measured immediately after suspension and 24 h later (figure 4 and supporting information (SI) S2). We did not observe a time dependent optical response (SI S2) but we did observe that the surface chemistry (*i.e.* the coating) had an influence on the performance of the sensor molecules.

Figure 4.A shows the whole vibrational pattern of the 4-MBA at different pH values recorded with the PEG coated sensor (AuNS@4-MBA@m-PEG). The intensity of the bands at 632, 695, 721, 801, 850, 1141, 1177, 1181, and 1422 cm<sup>-1</sup> varies at different pH values. As the pH increases, the band at 1422 cm<sup>-1</sup> becomes stronger and concentrates the most prominent changes that can be assigned to the carboxyl group dissociation (COO<sup>-</sup>), while the band at 1280 cm<sup>-1</sup> follows the opposite trend. Indeed, we could track the less prominent intensity variations at ~1280 cm<sup>-1</sup> related to the reduction of the concentration of the vibrational mode associated with the pH changes. Although we cannot associate a vibrational pattern to this band, Wei *et. al.*, also observed it.<sup>[35]</sup> Wei *et. al.*, also detected changes in the intensity of this band upon controlled agglomeration of the nanoparticles mediated by

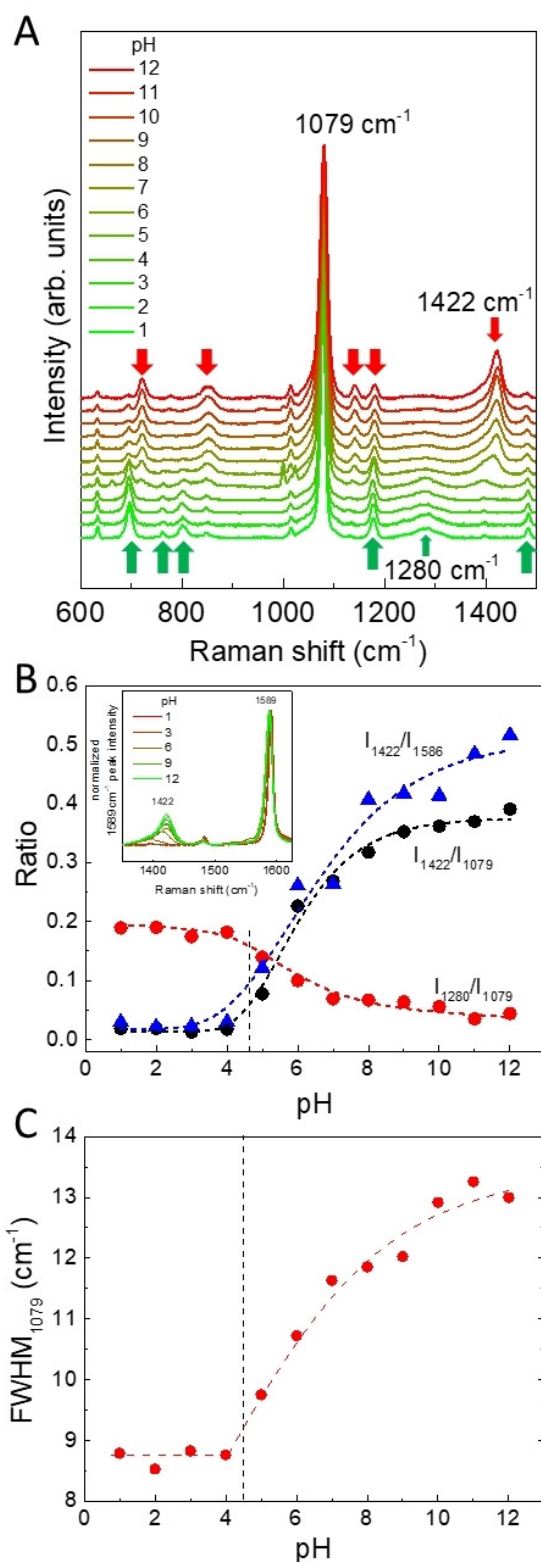


**Figure 4.** (A) SERS spectra recorded with AuNS@4-MBA@m-PEG in cell growth medium after 24 h. With red (green) arrows are marked the peaks that increase (decrease) the intensity with the increase of the pH (B) Calibration plots relating pH-sensitive and -insensitive intensity bands at  $1280\text{ cm}^{-1}/1079\text{ cm}^{-1}$  ( $I_{1280}/I_{1079}$ ),  $1422\text{ cm}^{-1}/1079\text{ cm}^{-1}$  ( $I_{1422}/I_{1079}$ ) and  $1422\text{ cm}^{-1}/1586\text{ cm}^{-1}$  ( $I_{1422}/I_{1586}$ ), respectively against pH. Inset shows the evolution of the Raman spectra region  $1350\text{--}1625\text{ cm}^{-1}$  normalized for the peak at  $1586\text{ cm}^{-1}$  (C) Correlation of the FWHM of the main band at  $1079\text{ cm}^{-1}$  with the pH.

changes in the solvent.<sup>[35]</sup> We think that the agglomeration of the nanoparticles created the required “hot spots” to increase the signal-to-noise ratio and amplify the signal at  $\sim 1280\text{ cm}^{-1}$  in a similar manner as we did. Strong pH-insensitive bands appear at  $1079\text{ cm}^{-1}$  and  $1586\text{ cm}^{-1}$  (SI S2.1 & 2.2) corresponding to aromatic ring vibrations of the 4-MBA. Additionally, an asymmetric band around  $1700\text{ cm}^{-1}$  (SI S2.1 & 2.2) appears to increase intensity at lower pH values due to the C=O stretching vibrations.<sup>[36–39]</sup>

The calibration curves (Figure 4.B) of the AuNS@4-MBA@m-PEG sensor response (ratio of the integrated areas under the different peaks considered) as a function of pH was further plotted. To this end, we took the pH-sensitive ( $1422\text{ cm}^{-1}$  and  $1280\text{ cm}^{-1}$ ) versus pH-insensitive band ( $1586\text{ cm}^{-1}$  and  $1079\text{ cm}^{-1}$ ) and made the ratio. Ratiometric measurements allow neglecting signal variations attributed to external parameters such as particle’s morphology, batch-to-batch or loading/uptake differences, etc. For the  $1280$  and  $1422\text{ cm}^{-1}$  bands, a detail analysis of the intensity dependence with the pH has been performed (Figure 4.B). The dependences show the presence of three different behaviors. For  $\text{pH} < 5$  the intensities ratio of the bands is constant associated with a pH threshold for the carboxyl group dissociation. For  $5 < \text{pH} < 8$  a clear dependence of the intensity ratio with the pH is observed, with higher sensitivity for the  $5 < \text{pH} < 8$  range and lower for  $\text{pH} > 8$  due to saturation effects. This dependence demonstrates the functionality in the physiological range is in agreement with the results reported by H. Wei *et al.*<sup>[35]</sup> The calibration curve (figure 4.B) has been fitted using a sigmoidal (Gompertz) curve, which is common in processes growing slowly at the start and at the end. The mathematical equation and fitting parameters are shown below (eq 1). A correlation coefficient of 0.988 indicates good agreement between the data values and the model applied.

$$\text{eq 1)} \quad I_{1422}/I_{1586} = 0.0196 + 0.4644e^{-e^{-0.6620 \cdot (\text{pH} - 5.5637)}};$$

$$r^2 = 0.988;$$

Additionally, in figure 4.C, we present the full width at half maximum (FWHM) of the dominant band at  $\sim 1079\text{ cm}^{-1}$  variations with respect to the pH. The FWHM is associated to energy dispersion of the energy vibration. The increase of this parameter is associated to increase of inhomogeneity in the distribution of different populations (protonated and non-protonated) of the 4-MBA molecule. This dependence provides an independent and complementary methodology for the assessment of the pH obtained without requiring additional experiments. Additionally, this methodology allows the use of the Raman measurements for the evaluation of the protonation of the molecule without the detection/evolution of the enhancement SERS bands at  $1280$  and  $1422\text{ cm}^{-1}$ .

These results demonstrate the fabrication of a functional colloidal pH meter (AuNS@4-MBA@m-PEG) that enables high quality SERS data to be obtained, providing a reliable SERS platform to perform pH bioanalysis.

On the contrary, no optical response was found for 4-MBA when using the AuNS@4-MBA@SiO<sub>2</sub> sensors (see SI) neither in the solutions (SI §2.2) nor inside the cells (SI §2.3). The lack of detection is due to an inefficient enhancement of the Raman signal due to the thickness of the silica shell that increases the interparticle distance and hinders the close contact of individual particles and the formation of “hot spots”. In such junctions, the enhancement is the highest<sup>[40–41]</sup> and leads to increased signal-to-noise ratios. This is crucial in any biomedical application because the presence of numerous macromolecules interfere with the target Raman signal. One could think of using silver, which is a better enhancer however, its associated toxicity limits the biomedical applications of this material. On one hand, the silica coating appeared to deliver a more sophisticated type of sensor with a fixed geometry<sup>[24,42]</sup> and with promising properties for biomedical applications. However, as said before, the thickness of a silica shell is responsible for an inefficient enhancement of the target Raman signal and therefore compromises the biofunctionality of this kind of sensors. On the other hand, a different coating such as the PEG for the same type of material showed good performances (Figure 4 and 5 and SI §2.1). Thus, indicating how important is

absorption wavelengths of individual nanoparticles are preferred. The presence of such nanoscale gaps between neighboring nanoparticles results in significant red-shift of the LSPR band from the visible to the NIR due to strong electromagnetic coupling effects. Additionally, gold has its characteristic electronic interband transitions in the visible range, therefore high wavelength laser lines are used. This “hot-spot” formation occurs upon interaction of the particles with the cells, either at the level of the cell membrane, where the particles accumulate before being engulfed or once inside the endocytotic vesicles. Figure 5.A shows an optical image of SK-BR-3 cells with AuNS@4-MBA@m-PEG (black dots) inside. SERS was performed over an extended area of the cell culture recording a total of 8531 SERS spectra and showing different signatures of 4-MBA that were color coded (fig. 5.B). The different colors represent different intensities for 1422 cm<sup>-1</sup> band and therefore, can be assigned to differences in the pH values of the surroundings. Red colored areas correspond to higher band intensity while the green corresponds to lower. For sake of clarity only one example of SERS spectra for each different area is shown in Figure 5.C presenting the aforementioned intensities variations. Local pH values were quantified (see Table 1) upon extrapolat-

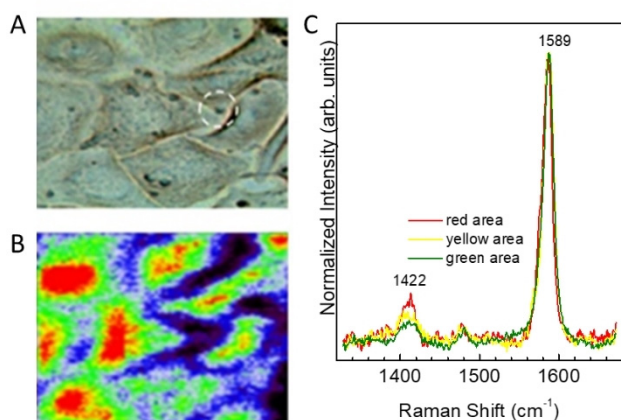


**Figure 5.** (A) Optical image of SK-BR-3 cells exposed to AuNS@4-MBA@m-PEG (dashed circle) after 24h. (B) Representation of pH map of the cells obtained by Renishaw StreamLine accessory. (C) Example of one recorded SERS spectrum for each coloured area. Spectrum of red areas shows higher SERS intensity for 1422 cm<sup>-1</sup> band and green the less. Areas under threshold are dark-coloured.

to correlate the physicochemical properties of nanoparticles with cellular responses to rationally design the configuration of the particles depending on the application.<sup>[43–45]</sup>

### pH sensing inside living cells

When the cells internalize the particles, they come in very close contact, the enhancement of weak Raman signals are highest due to the formation of “hot spots”, and bioanalysis is possible. However, it also explains why to excite effectively the AuNS, higher excitation wavelengths (785 nm) than the maximum

CELL AREAS	$I_{1422}/I_{1589}$	pH
RED	$0.304 \pm 0.005$	$7.00 \pm 0.25$
YELLOW	$0.268 \pm 0.002$	$6.56 \pm 0.25$
GREEN	$0.157 \pm 0.005$	$5.36 \pm 0.25$

ing the  $I_{1422}/I_{1589}$  to the calibration plot showed in the inset (Figure 5.C) using 1589 cm<sup>-1</sup> as the pH-insensitive band standard to perform the data analysis. The pH values for the red, yellow, and green areas were 7.0, 6.6 and 5.4, respectively, which indicate that the sensors have different locations. It is well known that the growth medium is slightly alkaline characterized by a pH 7–8, while the lysosomes have a more acidic pH of approx. 4–5. Intermediate vesicles of the endocytotic machinery have a pH of 5.5–7. In this way, particles showing a pH 7.0 are located outside the cells or onto cell membrane. Particles inside the cells showing lower pH values can be located inside the cells however, in different organelles of the endocytotic pathways as demonstrated by the different pH values (6.7, yellow areas and 5.4, green areas). These vesicles can be identified as early endocytic vesicles (pH 6.7) or endo/lysosomes (pH 5.4) as it is well known that the degree of acidification increases during endocytosis. This is in good agreement with the results obtained with the confocal microscope (figure 3), showing that SK-BR-3 cells internalize AuNS@4-MBA@m-PEG particles and are located inside endo/lysosomal organelles.

## Conclusions

In this work, we developed an optical pH nanoscale sensor able to reside inside eukaryotic cells as intracellular reporter. This sensor, with a SERS read out, is suitable for quantitative and localized pH sensing in real time. Sensing was performed along the way of internalization from the extracellular site through different endo/lysosomal compartments where they are closely packed. The creation of hot spots favored by particle agglomeration inside cells was responsible for the enhancement of changes in signal intensity and was dependent on the surface chemistry. Different coatings showed different sensing performances. Whereas too thick coatings like silica shells of around 20 nm impeded the formation of hot spots and signal detection, thinner layers around the particles like a corona of 1 kDa PEG molecules showed good performances. The presence of pH-sensitive and -insensitive bands facilitated ratiometric measurements and allowed that the read outs were independent from batch-to-batch differences, the degree of agglomeration, uptake or sensor loading. Furthermore, these optical sensors have the future capacity for multiplex detection of multiple ions. The SERS emission bands originated from each sensor molecule attached to a carrier are sharp and characteristic for each molecule, thus allowing spectral resolution of several ions in parallel.

## Supporting Information summary:

The Supporting Information (SI) file contains the complete Experimental Section and additional experimental data. In this work, we studied the effect of two different coatings for the biosensor on their sensing abilities along their cellular internalization. In the main manuscript, the key results related to the PEG coating are presented whereas additional data are shown in the SI. All information about the silica coating is presented in the SI.

## Acknowledgements

P.R.G. (RYC-2012-10059 and CTQ2013-45433-P), D. T. (FJCI-2015-26982) and M.S.S. (FJCI-2014-22398) acknowledge the Ministry of Economy, Industry, and Competitiveness (MINECO) for financial support.

## Conflict of Interest

The authors declare no conflict of interest.

**Keywords:** dynamic intracellular reporters · endocytosis · eukaryotic cells · ion sensing · live and real time biosensing · nanoscale optical sensors · surface enhanced Raman scattering

- [1] F. Lang, *J. Am. Coll. Nutr.* **2007**, *26*, 613S-623S.  
[2] M. J. Stutts, C. M. Canessa, J. C. Olsen, M. Hamrick, J. A. Cohn, B. C. Rossier, R. C. Boucher, *Science* **1995**, *269*, 847-850.  
[3] M. Mall, A. Hipper, R. Greger, K. Kunzelmann, *FEBS Lett.* **1996**, *381*, 47-52.

- [4] a) H. Matsui, B. R. Grubb, R. Tarran, S. H. Randell, J. T. Gatzky, C. W. Davis, R. C. Boucher, *Cell* **1998**, *95*, 1005-1015; b) G. K. Darbha, A. Ray, P. C. Ray, *ACS Nano* **2007**, *1*, 208-214.  
[5] A. M. Dolga, N. Terpolilli, F. Kepura, I. M. Nijholt, H. G. Knaus, B. D'Orsi, J. H. Prehn, U. L. Eisel, T. Plant, N. Plesnila, C. Culmsee, *Cell Death Dis.* **2011**, *2*, e147.  
[6] J. H. Viles, *Coord. Chem. Rev.* **2012**, *256*, 2271-2284.  
[7] R. Hohlfeld, *Nat. Med.* **2012**, *18*, 1743-1745.  
[8] P. Ehling, S. Bittner, T. Budde, H. Wiendl, S. G. Meuth, *FEBS Lett.* **2011**, *585*, 3836-3842.  
[9] M. Nazarenus, I. Abasolo, N. Garcia-Aranda, V. Voccoli, J. Rejman, M. Cecchini, S. Schwartz, P. Rivera Gil, W. J. Parak, *Part. Part. Syst. Character.* **2015**, *32*, 991-998.  
[10] E. Bakker, P. Buhlmann, E. Pretsch, *Chem. Rev.* **1997**, *97*, 3083-3132.  
[11] W. H. Tan, Z. Y. Shi, S. Smith, D. Birnbaum, R. Kopelman, *Science* **1992**, *258*, 778-781.  
[12] P. Buhlmann, E. Pretsch, E. Bakker, *Chem. Rev.* **1998**, *98*, 1593-1687.  
[13] I. L. Cameron, N. K. R. Smith, T. B. Pool, R. L. Sparks, *Cancer Res.* **1980**, *40*, 1493-1500.  
[14] S. Carregal Romero, J. M. Montenegro Martos, W. Parak, P. Rivera Gil, *Front. Pharmacol.* **2012**, *3*.  
[15] J. Peteiro-Cartelle, M. Rodriguez-Pedreira, F. Zhang, P. Rivera Gil, L. L. d. Mercato, W. J. Parak, *Nanomedicine* **2009**, *4*, 967-979.  
[16] D. Si, T. Epstein, Y.-E. Koo Lee, R. Kopelman, *Anal. Chem.* **2012**, *84*, 978-986.  
[17] A. Burns, P. Sengupta, T. Zedayko, B. Baird, U. Wiesner, *Small* **2006**, *2*, 723-726.  
[18] T. Nguyen, Z. Rosenzweig, *Anal. Bioanal. Chem.* **2002**, *374*, 69-74.  
[19] R. Ballerstadt, J. Schultz, *Anal. Chem.* **2000**, *72*, 4185-4192.  
[20] L. G. Dimosthenis, G. V. Athanasios, *Anal. Chim. Acta* **2011**, *683*, 156-169.  
[21] L. L. del Mercato, A. Z. Abbasi, M. Ochs, W. J. Parak, *ACS Nano* **2011**, *5*, 9668-9674.  
[22] a) J. Wang, *Chemical reviews* **2008**, *108*, 814-825; b) Z. Yue, W. Khalid, M. Zanella, A. Z. Abbasi, A. Pfreundt, P. Rivera Gil, K. Schubert, F. Lisdat, W. J. Parak, *Anal. Bioanal. Chem.* **2010**, *396*, 1095-1103.  
[23] A. Z. Abbasi, F. Amin, T. Niebling, S. Friede, M. Ochs, S. Carregal-Romero, J.-M. Montenegro, P. Rivera Gil, W. Heimbrod, W. J. Parak, *ACS Nano* **2011**, *5*, 21-25.  
[24] S. W. Bishnoi, C. J. Rozell, C. S. Levin, M. K. Gheith, B. R. Johnson, D. H. Johnson, N. J. Halas, *Nano Lett.* **2006**, *6*, 1687-1692.  
[25] a) L. Rodriguez-Lorenzo, Z. Krpetic, S. Barbosa, R. A. Alvarez-Puebla, L. M. Liz-Marzan, I. A. Prior, M. Brust, *Integr. Biol.* **2011**, *3*, 922-926; b) R. Perez-Pineiro, M. A. Correa-Duarte, V. Salgueirino, R. A. Alvarez-Puebla, *Nanoscale* **2012**, *4*, 113-116.  
[26] P. Rivera Gil, C. Vazquez-Vazquez, V. Giannini, M. P. Callao, W. J. Parak, M. A. Correa-Duarte, R. A. Alvarez-Puebla, *Angew. Chem., Int. Ed.* **2013**, *52*, 13694-13698.  
[27] K. L. Nowak-Lovato, B. S. Wilson, K. D. Rector, *Anal. Bioanal. Chem.* **2010**, *398*, 2019-2029.  
[28] J. Kneipp, H. Kneipp, B. Wittig, K. Kneipp, *Nano Lett.* **2007**, *7*, 2819-2823.  
[29] J. Kneipp, H. Kneipp, B. Wittig, K. Kneipp, *J. Phys. Chem. C* **2010**, *114*, 7421-7426.  
[30] A. Jaworska, L. E. Jamieson, K. Malek, C. J. Campbell, J. Choo, S. Chlopicki, M. Baranska, *Analyst* **2015**, *140*, 2321-2329.  
[31] S. Barbosa, A. Agrawal, L. Rodriguez-Lorenzo, I. Pastoriza-Santos, R. A. Alvarez-Puebla, A. Kornowski, H. Weller, L. M. Liz-Marzan, *Langmuir* **2010**, *26*, 14943-14950.  
[32] K. Van Hoecke, K. A. C. De Schampelaer, Z. Ali, F. Zhang, A. Elsaesser, P. Rivera Gil, W. J. Parak, G. Smagghe, C. R. Janssen, *Nanotoxicology* **2013**, *7*, 37-47.  
[33] C.-A. J. Lin, R. A. Sperling, J. K. Li, T.-Y. Yang, P.-Y. Li, M. Zanella, W. H. Chang, W. J. Parak, *Small* **2008**, *4*, 334-341.  
[34] F. Zhang, E. Lees, F. Amin, P. Rivera Gil, F. Yang, P. Mulvaney, W. J. Parak, *Small* **2011**, *7*, 3113-3127.  
[35] H. Wei, M. R. Willner, L. C. Marr, P. J. Vikesland, *Analyst* **2016**, *141*, 5159-5169.  
[36] C. E. Talley, L. Jusinski, C. W. Hollars, S. M. Lane, T. Huser, *Anal. Chem.* **2004**, *76*, 7064-7068.  
[37] J. Kneipp, H. Kneipp, B. Wittig, K. Kneipp, *J. Phys. Chem. C* **2010**, *114*, 7421-7426.

- [38] F. Wang, R. G. Widejko, Z. Yang, K. T. Nguyen, H. Chen, L. P. Fernando, K. A. Christensen, J. N. Anker, *Anal. Chem.* **2012**, *84*, 8013-8019.
- [39] A. Pallaoro, G. B. Braun, N. O. Reich, M. Moskovits, *Small* **2010**, *6*, 618-622.
- [40] R. A. Alvarez-Puebla, L. M. Liz-Marzan, *Small* **2010**, *6*, 604-610.
- [41] L. Brus, *Acc. Chem. Res.* **2008**, *41*, 1742-1749.
- [42] Y. Zhang, A. Manjavacas, N. J. Hogan, L. Zhou, C. Ayala-Orozco, L. Dong, J. K. Day, P. Nordlander, N. J. Halas, *Nano Lett.* **2016**, *16*, 3373-3378.
- [43] P. Rivera-Gil, D. Jimenez de Aberasturi, V. Wulf, B. Pelaz, P. del Pino, Y. Zhao, J. M. de la Fuente, I. Ruiz de Larramendi, T. Rojo, X. J. Liang, W. J. Parak, *Acc. Chem. Res.* **2013**, *46*, 743-749.
- [44] P. Rivera Gil, G. Oberdorster, A. Elder, V. Puentes, W. J. Parak, *ACS Nano* **2010**, *4*, 5527-5531.
- [45] K. Luyts, D. Napierska, B. Nemery, P. H. M. Hoet, *Environ. Sci.: Processes Impacts* **2013**, *15*, 23-38.

Submitted: May 18, 2017

Accepted: August 31, 2017